Letter

Petal formation law in a cellophane diaphragm subjected to a pressure difference

Gaku Fukushima,* Jun Hagiwara, Yusuke Nakamura, and Akihiro Sasoh
Department of Aerospace Engineering, Nagoya University, Furo-cho, Chikusa-ku, Nagoya 464-8603, Japan

(Received 29 March 2022; revised 12 July 2022; accepted 14 September 2022; published 17 October 2022)

In this study, a layer of cellophane, subjected to an air-pressure difference, was ruptured using a piercing needle. Accordingly, petal-like fragmentation was observed in the layer via high-speed imaging. Two types of crack-propagation regimes were subsequently observed experimentally. If a tensile stress lower than 20.6 MPa acted on the cellophane diaphragm, a single crack was generated, whose propagation speed was lower than that under higher-stress conditions. For tensile stresses greater than 23.7 MPa, the crack-propagation speed remained constant at approximately 0.86 km/s, even after altering the device size, pressure, and humidity on the low-pressure side. The number of cracks equidistant from the piercing point was expressed as a linear function of the tensile stress acting on the diaphragm.

DOI: 10.1103/PhysRevE.106.L043001

Introduction. Brittle materials may exist in the shape of a membrane [1], a glass plate [2], a shell [3], or a rod [4,5]. Their crack-propagation processes, resulting in fragmentation sizes and their distribution [6], play an important role. In particular, the fracture behavior of a layer of a tensioned diaphragm subjected to a gaseous pressure difference significantly depends on the material and other physical conditions. The foregoing still warrants further study. Moulinet and Adda-Bedia investigated the rupturing of highly stretched natural-rubber balloons—pierced by a blade or under spontaneous explosions [7]. They discovered that when the balloon's elastomeric diaphragm was under sufficient tensile stress, cracks propagated at a constant speed forming a treelike network. In contrast, the dynamic fracture of a tensioned diaphragm made of brittle materials is not yet well understood, despite its widespread use. As a typical example of such materials, cellulose films (cellophane) exhibit a highly brittle mechanical feature. Owing to this nature, a cellophane film is used for gas-separation diaphragms in shock tubes and shows favorable features for shock wave formation at a short distance [8–12]. In a previous study conducted by the authors of this paper [12], white sheets of a cellophane diaphragm were used in a shock tube. During the formation of petal-like fragmentation, the crack-propagation speed remained almost constant at approximately 0.8 km/s, irrespective of pressure differences. However, the previous research was conducted under limited conditions, and as such, the law of petal formation is still unclear. In the present study, such fragmentation caused by crack propagation is investigated by varying the experimental device size, pressure difference, and humidity. The petal formation law related to the dynamic fragmentation of a tensioned cellophane diaphragm is proposed based on the experimental results.

Experimental setup. A shock tube made of stainless steel with a square cross section was used for the experiment (Fig. 1). Two types of experimental setups, namely, I and II, were used for each size of the shock tubes. Duct A, a high-pressure channel with a diaphragm-rupture device, was used in both setups I and II. The diaphragm-rupture device comprised a pneumatic cylinder (SMC Co., CJ2B10-60AZ) to drive a needle, an electromagnetic valve (SMC Co., SY-3220), and a high-pressure air bottle. The needle had a cone with a diameter of 5 mm and an apex of 90°. The diaphragm rupture was initiated by an electrical signal from a pulse generator to the electromagnetic valve. Receiving the signal, air with about 0.7 MPa in the bottle was sent to the pneumatic cylinder so that the needle impinged on the cellophane diaphragm. At the same time, trigger signals were sent to a high-speed camera and a light source. Further information on the rupture device can be found in [11,12]. Duct B was used only in setup II. Two shock tubes with different square cross-sectional sizes D and lengths L were prepared for each setup. The values of D were equal in ducts A and B, where $D = 62$ and 120 mm; the lengths for duct A, L_A, were 515 and 1020 mm and those for duct B, L_B, were 515 and 1000 mm, respectively. In this research, a layer of a "white" cellophane film (Futamura Chemical Co. Ltd., PC5-W #300) with a thickness e of 21 μm was used to interface the high- and low-pressure gases. Unlike generally used, transparent cellophane film, the quality of visualizing the crack-propagation process was much improved with this coloring. The mechanical properties of the white cellophane film were largely similar to those of a plain (transparent) cellophane without any additives or surface coatings (Futamura Chemical Co. Ltd., PL #300); the differences in the measured tensile strength and elongation were approximately 6% and 4%, respectively. Therefore, the experiment was conducted using the white cellophane film; nevertheless, the results obtained in this research can be applied to plain cellophane as well. The white cellophane diaphragm was placed at the right end of duct A using a flange, and the gas in duct A was sealed with an O-ring. The initial pressures in ducts A and B are denoted as p_A and p_B, respectively. Duct A was supplied with dry, compressed air using a dryer and compressor

*fukushima.gaku.d8@s.mail.nagoya-u.ac.jp

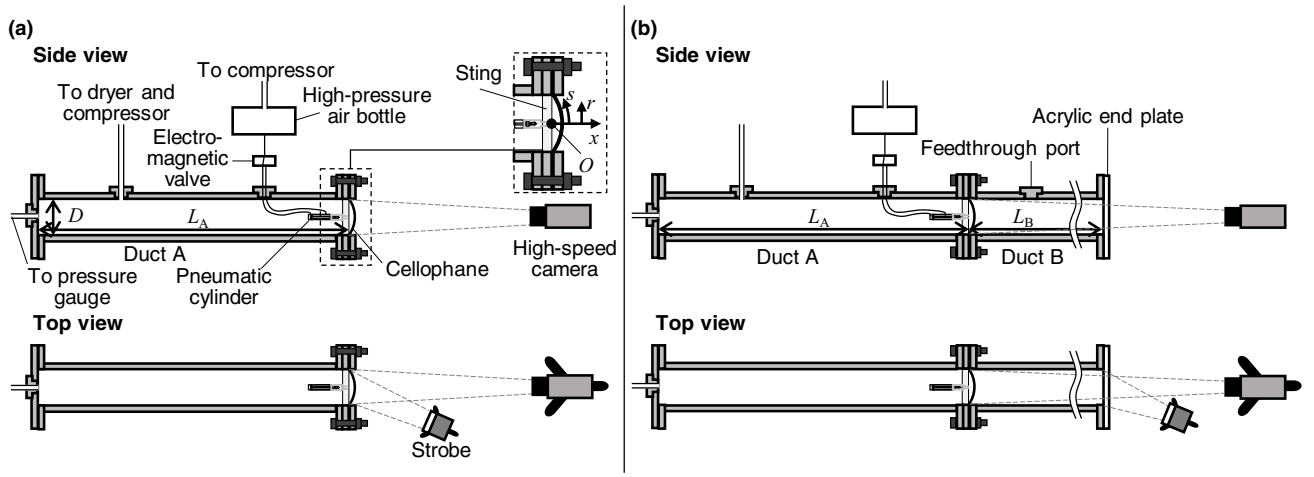

FIG. 1. Experimental setup. (a) Setup I for visualizing crack propagation. (b) Setup II for visualizing the complete opening process of the cellophane diaphragm in the shock tube. A strobe-light source is omitted in a side view.

through which atmospheric air was passed. The values of p_A and p_B were measured using a Bourdon gauge, and the reading error was 0.1 kPa. The temperature and relative humidity φ in the laboratory were recorded using a thermohygrometer just before the diaphragm was ruptured. The accuracies in the temperature and relative humidity were ± 1 K and $\pm 5\%$ RH (values shown in the product manual), respectively.

The origin O is set at a point along the diaphragm center before its bulge. The x axis is defined from the origin toward the right along the central axis of the ducts, and the y axis from the origin toward the depth direction of Fig. 1. The z axis points upward. The distance r is considered from the center axis [see Fig. 2(a)]. s is the arc length from the center axis on the bulged diaphragm.

Setup I, shown in Fig. 1(a), was used to capture the crack-propagation process during a relatively early stage of diaphragm rupture. The frame rate of the high-speed camera (Shimadzu Co., HPV-1) was set to 500 kfps (frame interval was 2 μs), and the exposure time was 1 μs. The positive region of the x axis is open to the laboratory in the atmospheric state. The diaphragm was illuminated by diffuse light from a strobe-light source (Panasonic, PE-60SG) placed slightly off axis to the center axis of the shock tube.

Setup II was used for capturing the opening motion of the petals of the ruptured diaphragm. The frame rate of the high-speed camera (Shimadzu Co., HPV-1 or NAC Image Technology Inc., Ultra Cam) was set to 32–40 kfps (time interval was 32–25 μs), and the exposure time was 3–16 μs. To replicate an actual shock tube operation, duct B was installed on the low-pressure side. A transparent acrylic end plate was installed at the end of duct B. Because the feedthrough port on the top surface of duct B was kept open until just before the diaphragm was ruptured, the initial conditions of the gas in duct B were equivalent to those of the laboratory atmosphere (pressure, temperature, and humidity), as in setup I. For setup II, the same strobe-light source was used as in setup I.

Experimental results and discussion. The deformation of the cellophane diaphragm was measured under different conditions of p_A and φ in setup I. The measurement results revealed that the diaphragm was deformed into an almost spherical shape. Thus, the displacement at the center of the diaphragm (on the x axis) was measured, and the spherical shape was obtained by assuming a zero displacement at $(y, z) = (0, \pm D/2)$ and $(\pm D/2, 0)$. The bulge at the center of the diaphragm x_0 was found to vary depending on the pressure difference and humidity on the low-pressure side: It increased with humidity for the same pressure difference and with the pressure difference for the same humidity on the low-pressure side. This trend is consistent with the technical data provided by the cellophane manufacturer on the mechanical properties of cellophane: The elongation of the cellophane diaphragm increases with the relative humidity, and the tensile strength decreases [13]. If the compressibility of the material is

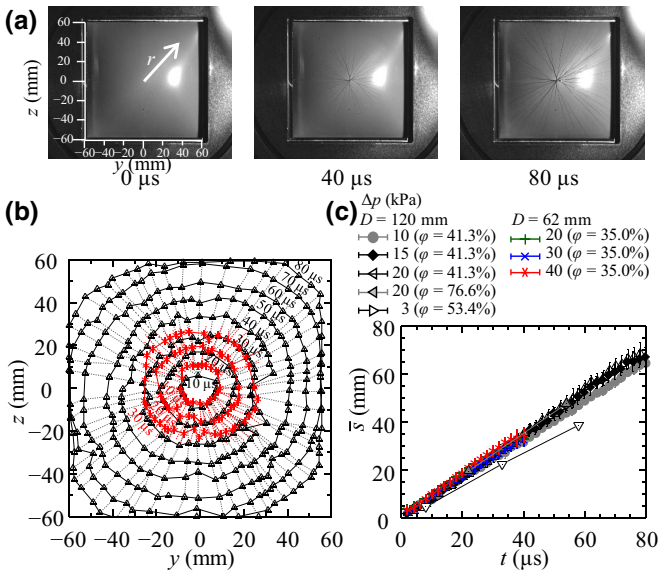

FIG. 2. Crack-propagation behaviors. (a) Sequential images of crack evolution at $p_A = 121.5$ kPa and $p_B = 101.5$ kPa. (b) Time evolution of the crack-front locations at $(D, \Delta p, \varphi) = (120$ mm, 20 kPa, 41.3% RH) (black triangle) and (62 mm, 40 kPa, 35% RH) (red cross). (c) Time evolution of the averaged crack length $\bar{s}$. Symbols are the same in (b), (c).

ignored, the strain of the diaphragm can be estimated as the ratio of the stretched length to that in the original state. In this study, the minimum strain value was 0.011, and the maximum was 0.42. In a previous study [7], the strain value was found to be 7.0 ± 0.5 for natural rubber, indicating that the cellophane diaphragm used in this study is more brittle. The tensile stress σ_i (Pa) acting on a partial spherical shell under a pressure difference $\Delta p (= p_A - p_B)$ was calculated using the following equation:

$$\sigma_i = \frac{\Delta p R}{2e}, \tag{1}$$

where R is the radius of curvature of the partial spherical shell computed from x_0. The error contained in σ_i, estimated by the measurement error of x_0 and Δp, is approximately 2%.

Examples of sequence images and animations for the crack propagation in setup I are shown in Fig. 2(a) and in the Supplemental Material [14]. The pressure, humidity, and temperature were set as follows: $p_A = 121.5$ kPa, $p_B = 101.5$ kPa, $\varphi = 41.5\%$ RH, and 292.9 K. The calculated tensile stress was $\sigma_i = 54.8$ MPa. The frame just before the first crack was identified and set to $t = 0$ μs. The time t had an uncertainty of 2 μs owing to the frame interval. The crack propagated from the center of the diaphragm immediately after needle impingement. As the distance from the origin increased, crack branching was observed. Details regarding the branching events will be discussed later.

Figure 2(b) illustrates plots of the crack-front positions extracted from sequential images captured after every 10 μs under two different conditions. The results corresponding to $D = 62$ mm have already been reported in a previous paper [12]. The conditions of tensile stress were approximately equivalent to each other ($\sigma_i = 54.8$ and 54.1 MPa). The propagation speed of the crack front under the two different conditions remained unchanged. Figure 2(c) depicts the time evolution of the averaged crack front location on the arc, expressed as $\bar{s}$. Influences of the differences in the shock-tube scale, pressure, and low-pressure section humidity on the crack-propagation speed were examined. For $\varphi = 53.7$, 76.6% RH, and $D = 120$ mm, the experimental results in setup II were used. As the time resolution was 32 or 25 μs during this setup, the time t was synchronized by comparing the images of the first crack appearance with the result obtained under the same pressure difference but different humidity. As shown in Fig. 2(a), because there exists a saturated region of brightness on the right-hand side of the diaphragm ($20 < y < 40$), $\bar{s}$ is calculated using the crack fronts in $y < 0$. $\bar{s}$ increases linearly with time: The speed of the cracks is constant. In the low-pressure condition ($\Delta p = 3.0$ kPa), a single crack is generated [later shown in Fig. 3(a) $\sigma_i = 20.0$ MPa], and the crack-propagation speed is lower than that under the other condition (619 m/s). Under other conditions, multiple cracks are generated, and the crack front propagation speed is constant regardless of D, Δp, and φ. The average speed is 855 ± 37 m/s. This speed should be compared with the longitudinal- and shear-wave speeds. Herein, we quantitatively estimate the longitudinal- and shear-wave speeds of cellophane. These speeds can be calculated using the Young's modulus E and Poisson's ratio ν of the material by assuming a bulk. The longitudinal-wave speed can be expressed as $\sqrt{E(1-\nu)/\{\rho(1+\nu)(1-2\nu)\}}$, and the shear-wave speed can be expressed as $\sqrt{E/\{2\rho(1+\nu)\}}$, where $\rho (= 1460\,\mathrm{kg/m^3})$ is the mass density of cellophane. According to the cellophane manufacturer, the value of E for cellophane with a humidity of approximately 60% RH is $E \approx 4.42$ GPa. However, we also obtained a value of $E \approx 3.2$ GPa from the elastic range in the stress-strain curve (0.25% stretch at 80 MPa) presented in [15]. We also assumed υ to be 0.3−0.4, similar to that of other polymer materials. Consequently, the longitudinal-wave speed was estimated to be 2269−2806 m/s using $E \approx 4.42$ GPa and 1930−2387 m/s using $E \approx 3.2$ GPa. Additionally, the shear-wave speed was estimated to be 1402−1455 m/s using $E \approx 4.42$ GPa and 1194−1239 m/s using $E \approx 3.2$ GPa. Therefore, the difference of 1.2 GPa in the value of E obtained via the two approaches caused a difference of 339−419 m/s in the longitudinal-wave speed and a difference of approximately 200 m/s in the shear-wave speed. We can conclude that the crack-propagation speed obtained in the experiment was approximately 30%–38% of the longitudinal- and 59%–61% of the shear-wave speeds, if we employed the value stated in the manufacturer's data (36%–44% of the longitudinal- and 69%–72% of the shear-wave speed if we use the value from Ref. [15]). Previous studies have shown that the crack-propagation speed is constant during explosions of highly tensioned natural rubber [7] and cellophane [12] for a single length scale of the facility length. In this study, it is confirmed that the crack-propagation speed is constant even when the facility length, pressure difference, and humidity on the low-pressure side are altered.

Figure 3(a) and the Supplemental Material [14] illustrate examples of the opening process of the cellophane diaphragm visualized using setup II. The temperature in duct B ranges from 289.6 to 295.0 K. The humidity φ in duct B is different in each experiment, within 20.0% RH $\leqslant \varphi \leqslant$ 76.6% RH. The humidity affects the initial deformation of the diaphragm, which changes the initial tensile stress acting on the diaphragm, σ_i. The calculated values of σ_i are within $0\,\mathrm{MPa} \leqslant \sigma_i \leqslant 68.7\,\mathrm{MPa}$. The small tensile stress ($\sigma_i \leqslant 10.3$ MPa) is obtained by the following pressure setting process: applying $p_A = p_B + 20.0$ kPa, and then, decreasing it to $p_A \leqslant p_B + 3.0$ kPa. Because the diaphragm undergoes a partial plastic deformation owing to the pressure difference, we obtain a small Δp and R in Eq. (1) by following the aforementioned procedure and examine the small tensile stress condition. The time t is synchronized by comparing the images of the first crack appearance to images captured every 2 μs in the previous experiment [Fig. 2(a)]. As shown in Fig. 3(a), two types of crack-propagation regimes are observed. When $\sigma_i = 3.45$ and 20.0 MPa, a single crack is generated, while a crack branch cannot be observed. Moreover, in the lowest tensile stress case ($\sigma_i = 3.45$ MPa), we discover that the crack propagation stops before reaching the duct wall. Alternatively, in higher tensile stress cases ($\sigma_i \geqslant 25.9$ MPa), petal-like fragments are formed by crack propagation with branching from the center of the diaphragm, and they begin rotating about the axis of rotation on the wall. The number of petals varies with σ_i. Under high tension, $\sigma_i = 68.7$ MPa, a large number of petals is formed (146 petals), and the apex angle of the petals becomes extremely small. On the contrary, a smaller tensile

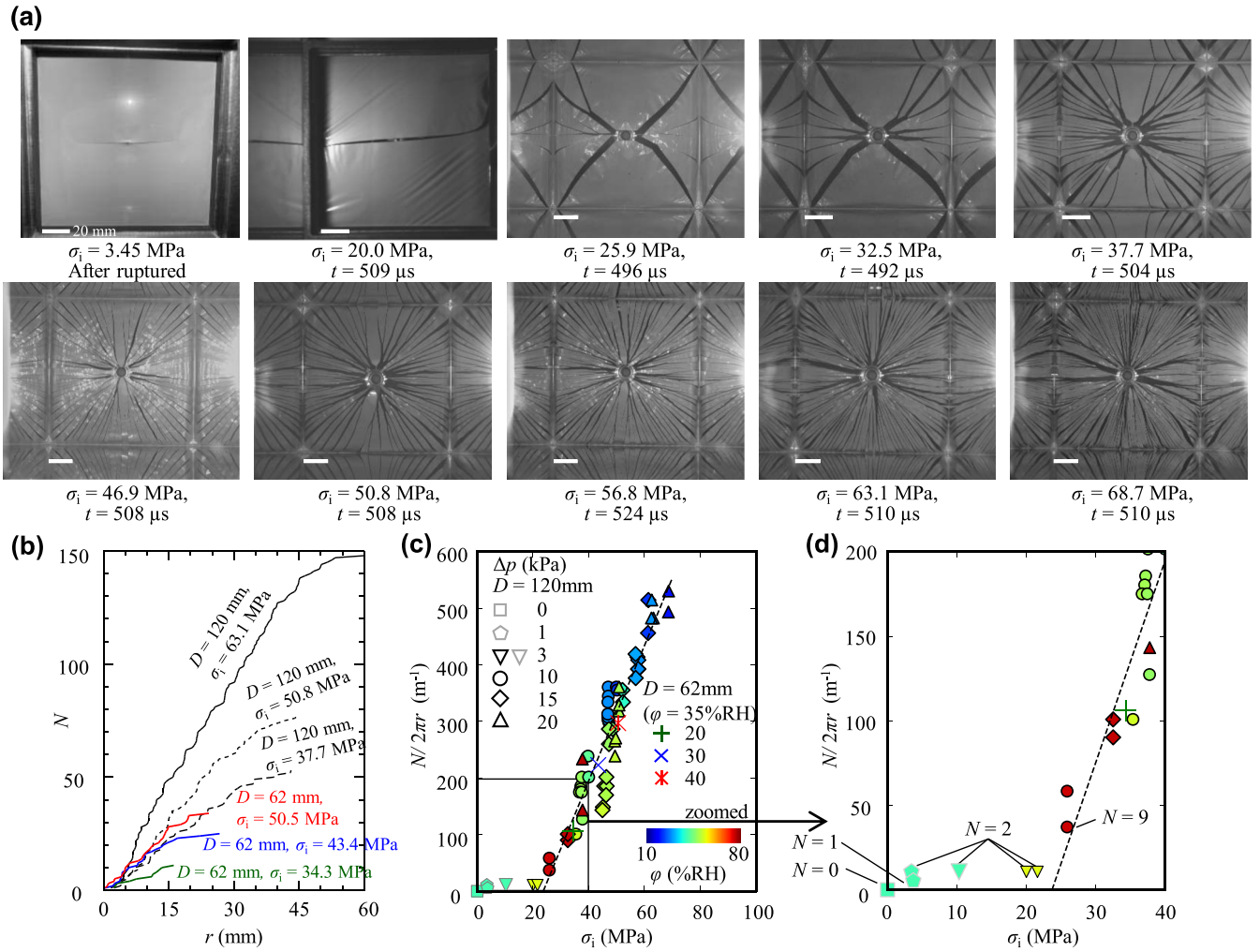

FIG. 3. (a) Examples of the diaphragm-ruptured morphology under different humidity values at different σ_i in setup II. Brightness and contrast are adjusted for visibility. (b) Number of cracks N as a function of r. (c), (d) $N/2\pi r$ vs σ_i, where the dotted line represents the linear fitting results for all the plots wherein crack branch events are observed. The plots $\sigma_i \leqslant 10.3$ MPa (with gray plot frames) correspond to the experimental condition wherein p_A is decreased to $p_A \leqslant p_B + 3.0$ kPa after it had been $p_A = p_B + 20.0$ kPa. The line colors in (b) and plot colors in (c) for $D = 62$ mm are the same.

stress results in a smaller number of petals. The number of petals is 9 when $\sigma_i = 25.9$ MPa. Notably, the aforementioned two types of crack-propagation regimes have been observed in a previous study for a highly elastomeric material [7]; however, in this study, we discovered the observation of similar crack-propagation regimes for a highly brittle material.

Figure 3(b) shows the variation in the number of crack fronts N with respect to the coordinate r obtained from the image. For clear detectability of the petal tips, the image in the range of $100\,\mu s < t < 200\,\mu s$ is used for $D = 120$ mm. The detected branch position (petal tip position) is different from the initial branch points by approximately 3 mm at most. This is because the central area begins to exhibit rotational motion earlier than the marginal area. For $D = 62$ mm, the postmortem cellophane diaphragm after the experiment was used in the analysis. With increasing r, N increased almost linearly. This trend indicates that the crack grows, keeping a certain constant difference from neighboring cracks. When r exceeded $D/4$ (30 and 15.5 mm for $D = 120$ and 62 mm, respectively), the rate of increase in N decreased compared with that for $r < D/4$.

The subsequent paragraphs present a discussion on the number of cracks formed. We examine the number of crack fronts equidistant from the origin, which are induced by needle impingement, by using $N/2\pi r(\mathrm{m}^{-1})$. To count of the number of cracks, the region $r \leqslant D/4$ is used, where N linearly increases with r as shown in Fig. 3(b). In this region, boundary reflections are not relevant according to the above stated estimations of longitudinal- and shear-wave speeds. Figure 3(c) shows a plot of $N/2\pi r$ as a function of the initial diaphragm tensile stress σ_i. The greatest value of $N/2\pi r$ was 531 m^{-1} when $\sigma_i = 68.7$ MPa. If we assume that the cracks were generated equidistantly, the crack grew, keeping a constant distance of 1.88 mm from neighboring cracks in this condition. On the contrary, the smallest value was 47.7 m^{-1} when $\sigma_i = 25.9$ MPa, and the distance between cracks was estimated to be 20.9 mm. For conditions wherein crack branch events are observed ($\sigma_i \geqslant 25.9$ MPa), the relation between

$N/2\pi r$ and σ_i can be fitted using a linear function, as follows:

$$N/2\pi r = \alpha(\sigma_i - \sigma_c), \tag{2}$$

where α and σ_c are fit to constant values of $1.20 \times 10^{-5}\,\mathrm{Pa^{-1}\,m^{-1}}$ and 23.7 MPa, respectively. The determination coefficient is 0.859. We can consider that $\sigma_c = 23.7\,\mathrm{MPa}$ is the threshold stress of the crack branch in the cellophane diaphragm. This petal formation law is derived from the experimental results of the different device scales D and humidity φ. Therefore, the petal formation law in Eq. (2) is a single function of σ_i, which means that the distance between cracks can be quantitatively estimated by σ_i. Thus, this law enables us to predict fragmentation behaviors of the cellophane diaphragm in application situations, for example, shock tube operations. Alternatively, when σ_i is smaller than σ_c, the cracks exhibit a different behavior from that of the high-stress case. In a magnified plot of Fig. 3(c), the behavior of $N/2\pi r$ under a low stress can be observed. When $\sigma_i \leqslant 20.6\,\mathrm{MPa}$, crack branch events cannot be observed ($N = 2$). Under the condition of lower σ_i, the single crack does not reach the shock tube wall. When $\sigma_i = 3.71\,\mathrm{MPa}$, the right-side tip of the single crack stops at $r < D/4$, and $N = 1$. When the tensile stress is zero, the needle simply penetrates the diaphragm without leading to crack propagation ($N = 0$). The present experiment clarifies that $N/2\pi r$ is significantly influenced by σ_i. If σ_i is higher than a certain minimum value (25.9 MPa in this experiment), crack branching events occur, and $N/2\pi r$ follows Eq. (2). If σ_i is smaller than a certain maximum value (20.6 MPa in this experiment), a single crack is generated. Moreover, when σ_i is smaller than 3.71 MPa, crack propagation stops prior to the wall.

Conclusions. In summary, we experimentally investigated crack-propagation behavior in a layer of cellophane diaphragm subjected to a pressure difference. We observed two types of crack-propagation regimes depending on the tensile stress acting on the cellophane diaphragm. When the tensile stress was lower than 20.6 MPa, a single crack was generated, whose propagation speed was lower than that under high-stress conditions. When the tensile stress was larger than 25.9 MPa, on the contrary, the crack-propagation speed exhibited a constant value of 855 m/s, even when the facility size, pressure difference, and humidity on the low-pressure side were varied. This speed was 30%–46% of the longitudinal-wave speed and 59%–72% of the shear-wave speed. Further, we deduced the following experimental law: The number of crack fronts per circumferential length becomes a linear function of only the initial tensile stress.

Acknowledgments. The authors would like to acknowledge Futamura Chemical Co. Ltd. for kindly donating the cellophane film. We appreciate Kiyoshi Kinefuchi for helpful comments, and Jiaxi Wei and Shingo Ogawa for their experimental assistance. We also thank Akira Saito and the staff members at the technical division of Nagoya University for their technical assistance. This research was supported by JSPS KAKENHI (Grants No. JP18H03813, No. JP21H04589, and No. JP21J15243).

[1] J. Åström and J. Timonen, Phys. Rev. Lett. **79**, 3684 (1997).
[2] N. Vandenberghe, R. Vermorel, and E. Villermaux, Phys. Rev. Lett. **110**, 174302 (2013).
[3] F. Wittel, F. Kun, H. J. Herrmann, and B. H. Kröplin, Phys. Rev. Lett. **93**, 035504 (2004).
[4] J. R. Gladden, N. Z. Handzy, A. Belmonte, and E. Villermaux, Phys. Rev. Lett. **94**, 035503 (2005).
[5] E. Villermaux, K. Keremidis, N. Vandenberghe, M. J. Abdolhosseini Qomi, and F.-J. Ulm, Phys. Rev. Lett. **126**, 045501 (2021).
[6] S. Kooij, G. van Dalen, J. F. Molinari, and D. Bonn, Nat. Commun. **12**, 2521 (2021).
[7] S. Moulinet and M. Adda-Bedia, Phys. Rev. Lett. **115**, 184301 (2015).
[8] T. Ikui and K. Matsuo, Bull. JSME **12**, 774 (1969).
[9] T. Ikui, K. Matsuo, and M. Nagai, Bull. JSME **12**, 783 (1969).
[10] B. D. Henshall, Aeronautical Research Council, Reports and Memoranda, No. 3044, 1955.
[11] T. Tamba, T. M. Nguyen, K. Takeya, T. Harasaki, A. Iwakawa, and A. Sasoh, Shock Waves **25**, 667 (2015).
[12] G. Fukushima, T. Tamba, A. Iwakawa, and A. Sasoh, Shock Waves **30**, 545 (2020).
[13] Futamura Chemical Co. Ltd. (private communication, December 2021).
[14] See Supplemental Material at http://link.aps.org/supplemental/10.1103/PhysRevE.106.L043001 for animations of the crack propagation and the cellophane diaphragm opening process.
[15] B. Zhang, J. Azuma, and H. Uyama, RSC Adv. **5**, 2900 (2015).